

Lifshitz transition in the double-core vortex in $^3\text{He-B}$

M. A. Silaev,¹ E. V. Thuneberg,² and M. Fogelström³

¹*Department of Theoretical Physics, KTH-Royal Institute of Technology, SE-10691 Stockholm, Sweden*

²*Department of Physics, University of Oulu, FI-90014, Finland*

³*Department of Microtechnology and Nanoscience, Chalmers, SE-41296 Göteborg, Sweden*

(Dated: December 7, 2015)

We study the spectrum of fermion states localized within the vortex core of a weak-coupling p-wave superfluid. The low energy spectrum consists of two anomalous branches that generate large density of states at the locations of the half cores of the vortex. Fermi liquid interactions significantly stretch the vortex structure, which leads to Lifshitz transition in the effective Fermi surface of the vortex core fermions. We apply the results to rotational dynamics of vortices in superfluid $^3\text{He-B}$ and find explanation for the observed slow mode.

PACS numbers: 67.30.he, 67.30.hj, 74.25.nj

The double-core vortex is an amazing structure because it is the unique answer to a simple question: what is the vortex structure of a weak-coupling p-wave-pairing superfluid. The ground state in this case is the Balian-Werthamer (BW) state [1]. The lowest energy vortex has the double-core structure, where the core is split into two “half cores” as depicted in Fig. 1(a,b) [2–8]. This is not only of theoretical interest since superfluid ^3He is close to being weak coupling, and its B phase was identified as the BW state. Two vortex types have been found experimentally in $^3\text{He-B}$ [9–12]. The vortex being stable in the major, low-pressure part of the phase diagram was identified as the double-core vortex. The vortex stable at higher pressures was identified as the axially symmetric A-phase-core vortex. Available experimental evidence is consistent with the theoretical identification of the vortex structures. In particular, the broken axial symmetry of the double-core vortex was used to explain the peculiar dynamical properties that have been observed for the low pressure vortex using homogeneous precessing domain (HPD) mode of NMR [13, 14]. A similar double-core vortex structure has been suggested to appear in spin-triplet heavy fermion superconductor UPt_3 [15].

One of the most interesting properties of quantized vortices in superconductors and Fermi superfluids is the presence of fermionic quasiparticles localized within vortex core at energies smaller than the bulk energy gap [16, 17]. Generally fermionic bound states determine both thermodynamic and dynamic properties of vortices at low temperatures [18–22]. In the rotational dynamics of the double-core vortex they are predicted to give rise to resonance absorption at the frequency comparable with the spacing of the localized energy eigenstates [23]. Recently much attention has been focused on the topologically protected zero energy vortex-core and surface states in superfluid ^3He [24–27]. Particularly motivating is a predicted existence of self-conjugated Majorana states localized on half-quantum vortices in p-wave superfluids [28].

In this letter we calculate the low-energy fermionic excitation spectrum of the double-core vortex. We find that the low-energy excitations mostly are localized in the two

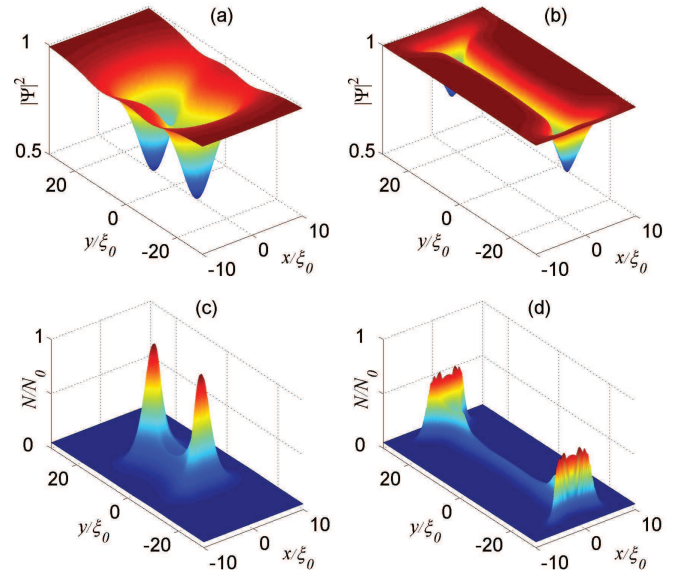


FIG. 1: (Color online) (a,b) The double-core vortex structure made visible by the pair density $|\Psi|^2 = \sum_{\mu,i} |A_{\mu,i}|^2$ plotted in the $x-y$ plane perpendicular to the vortex axis at temperature $T/T_c = 0.9$, and (b) $T/T_c = 0.1$. (c,d) The normalized local density of states profiles demonstrating the quasiparticle wave function at the Fermi level $\varepsilon = 0$, $\hat{p}_z = 0$ at $T/T_c = 0.9$ and (d) $T/T_c = 0.1$. All plots correspond to pressure $P = 24$ bar.

half cores. This is visualized in Fig. 1(c,d) which show the fermionic local density of states (LDOS) profiles around the vortex core. We can interpret the two half cores as potential wells for quasiparticles. The motion of the excitations between the wells depends on the potential barrier between them. We find that this barrier changes essentially as the distance of the wells changes as a function of pressure and temperature (see Fig. 1 to compare vortex structures at $T/T_c = 0.9$ and $T/T_c = 0.1$). This implies a transition from excitations that circle both half cores to separate excitations that circle only a single half core. This transition can be seen as a Lifshitz-type transition in the topology of the fermionic states bound to

the vortex core. We discuss how this could be observable in the time scales of rotational dynamics. Comparing our calculations with an earlier experiment reveals a serious disagreement in the model used to interpret the experimental data [14]. We construct a different model, which also provides an explanation for the long time scale observed in rotational dynamics [13, 29, 30].

The triplet pairing of fermions in orbital p -wave states is described by the matrix

$$\tilde{\Delta}(\mathbf{r}, \hat{\mathbf{p}}) = \sum_{\alpha, i} A_{\alpha i}(\mathbf{r}) i \tilde{\sigma}_\alpha \tilde{\sigma}_y \hat{p}_i, \quad (1)$$

where $\tilde{\sigma}_{x,y,z}$ are Pauli matrices, \mathbf{p} is the momentum close to the Fermi surface $p \approx p_F = \hbar k_F$, and $\hat{\mathbf{p}} = \mathbf{p}/p$. The gap function $\tilde{\Delta}$ (1) is determined by the 3×3 order parameter matrix with complex components $A_{\alpha i}$. Here $\alpha = x, y, z$ and $i = x, y, z$ are spin and orbital indices, respectively.

In the weak coupling theory of p -wave superfluid, the stable state has the Balian-Werthamer (BW) form [1]. In BW state, the order parameter far from the vortex axis is $A_{\alpha i} = \Delta_0 \exp(i\varphi) R_{\alpha i}$. Here φ is the azimuth with respect to the vortex axis, $R_{\alpha i}$ is a constant rotation matrix and Δ_0 the order parameter amplitude. Near the vortex axis a more sophisticated structure appears [2–8]. It is energetically favorable to change the sign of the order parameter across the vortex axis by spin rotation of the BW-state matrix $A_{\alpha i}$ by π [4]. This effectively results in splitting of a singly-quantized vortex to a pair of half-quantum vortices that are bound together by a planar-phase domain wall. For illustration see Figs. 1(a) and 1(b), which show the pair density $|\Psi|^2 = \sum_{\alpha, i} |A_{\alpha i}|^2$ in the $x - y$ plane. The pair density has two distinct minima, whence the name double-core vortex.

To determine the vortex structure we calculate self-consistently the order parameter and the Fermi-liquid self energy [31]. The numerics is performed as described in Ref. 6, i.e. using the explosion trick to solve the Eilenberger transport equation. We extend the previous work [6, 7] to higher accuracy, lower temperatures and different values of the Fermi-liquid parameter F_1^s corresponding to different pressures. The parameter F_1^s determines the feedback of superfluid mass current on the order parameter and can significantly change both the vortex structure and spectrum of bound fermions.

The distance a between the half cores is shown Fig. 2. Its scale is $R_0 = (1 + F_1^s/3) \xi_0$, where $\xi_0 = \hbar v_F / 2\pi T_c$ is the coherence length and v_F the Fermi velocity. As F_1^s in liquid ^3He ranges from 5.4 to 14.6 depending on pressure P [32], the two length scales can differ essentially. Thus at large values of F_1^s , corresponding to high pressures, the vortex size at a low temperature is much larger than the coherence length. For example, $a = 46\xi_0$ in the case of Fig. 1(b). Fig. 2 also shows strong temperature and pressure dependence. The distance of the half cores grows almost 3-fold when the temperature decreases from $0.9T_c$ to $0.1T_c$ at 24 bar. Similarly as a function of pressure the distance a measured in units of ξ_0 , grows almost

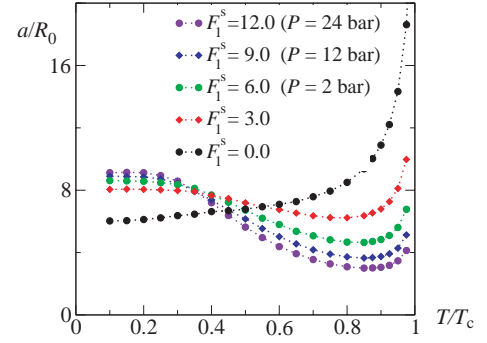


FIG. 2: (Color online) Distance a between the half cores in the double-core vortex at different values of the Fermi liquid parameter F_1^s . The locations of the half cores are determined from zeros of supercurrent density.

2-fold when the pressure increases from 0 to 24 bar at a low temperature.

We calculate the excitation spectrum of the double-core vortex using the self-consistent order parameter field. This is done by solving the eigenvalue problem for the system of Andreev equations, which are ordinary differential equations describing the propagation of quasiparticle wave function along classical trajectories.

The momentum \mathbf{p} of a low energy excitation is close to the Fermi surface, $p \approx p_F$. The classical trajectories are straight lines parallel to \mathbf{p} . In studying a vortex we fix the z axis as the vortex axis, and we parameterize the momentum direction $\hat{\mathbf{p}} = (\hat{p}_\perp \cos \theta_p, \hat{p}_\perp \sin \theta_p, \hat{p}_z)$. The direction on the trajectory is fixed by giving \hat{p}_z and θ_p . The location of the trajectory is given by the impact parameter b , the coordinate measuring the distance from the vortex axis. The parameterization is visualized in Fig. 3(a). The impact parameter is related to the projection of the angular momentum μ on the vortex axis through the usual classical mechanics formula $\mu = p_\perp b$. The quasiclassical energy spectrum is given by $\varepsilon = \varepsilon_i(\hat{p}_z, \theta_p, b)$, where the parameters \hat{p}_z, θ_p, b specify the classical trajectory and integer i counts the eigenvalues of Andreev equations on a given trajectory [33]. Figure 3(b) shows a bunch of trajectories at the Fermi level and $\hat{p}_z = 0$. The concentration of the trajectories at the two half cores results in the large LDOS at the half cores. The concave triangular shape of the caustic of the trajectories at the half cores is clearly visible in the LDOS shown in Fig. 1(d). Also the classically non-allowed region around the vortex axis in Fig. 3(b) can be recognized in Fig. 1(c) as a valley in the LDOS profile in the region between the half cores.

Due to the lifted spin degeneracy, singly-quantized vortices in $^3\text{He-B}$ have two anomalous branches of quasiparticle spectrum [34]. At low energy compared to the bulk energy gap, $|\varepsilon| \ll \Delta_0$, they can be represented as

$$\varepsilon_i(\hat{p}_z, \theta_p, b) = -\omega_i p_F (b - b_i), \quad (2)$$

where $i = 1, 2$. Here $b_i(\hat{p}_z, \theta_p)$ is the impact param-

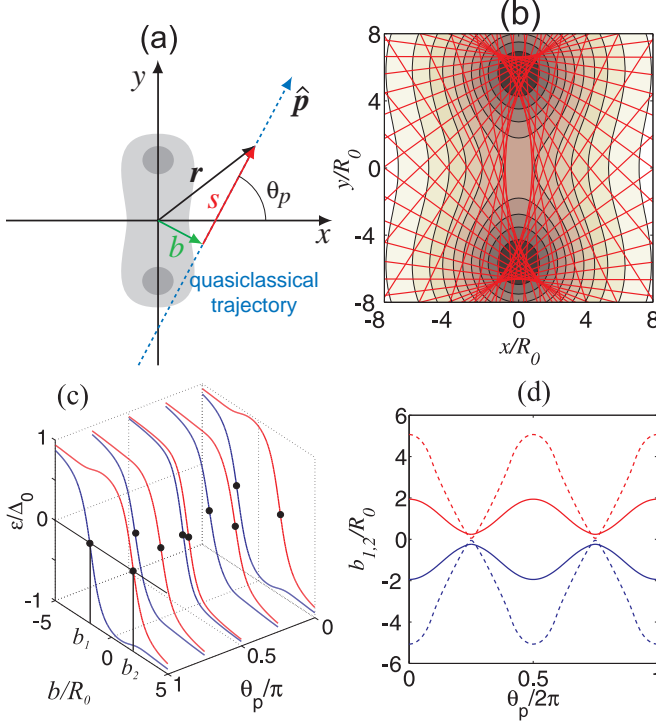


FIG. 3: (Color online) (a) Schematic plot of a quasiclassical trajectory in the $x-y$ plane in the direction of $(\cos \theta_p, \sin \theta_p)$ passing the vortex axis at distance b (impact parameter). A point $\mathbf{r} = (x, y)$ on the trajectory is determined by the coordinate s . (b) A bunch of quasiparticle trajectories (straight lines) at the Fermi level $\varepsilon = 0$ and $\hat{p}_z = 0$ superimposed on the pair-density contour plot at $T/T_c = 0.5$ and $F_1^s = 0$. (c) Anomalous branches of the quasiparticle spectrum $\varepsilon = \varepsilon_{1,2}(b, \theta_p)$ at $\hat{p}_z = 0$, $F_1^s = 12$ and $T = 0.9T_c$. (d) Two sheets of effective Fermi surface $b = b_{1,2}(\theta_p)$ at $\hat{p}_z = 0$, $F_1^s = 12$, $T = 0.9T_c$ (solid lines) and $T = 0.1T_c$ (dashed lines).

ter that corresponds to vanishing excitation energy, and $\omega_i(\hat{p}_z, \theta_p)$ indicates the slope of the energy at $b = b_i$. The new feature in a non-axisymmetric vortex is that these parameters depend on the trajectory direction θ_p in the $x-y$ plane.

Fig. 3(c) shows the calculated quasiparticle energies as a function of impact parameter b and different directions of the trajectory θ_p . The curves cross the Fermi level at a finite b in accordance with Eq. (2). These locations in the energy spectrum $b_{1,2}(\theta_p)$ are shown by the black dots in Fig. 3(c). The states at the Fermi level in the spectrum (2) form a 2D *effective Fermi surface* $b = b_{1,2}(\hat{p}_z, \theta_p)$ in the 3D space formed by the quasiclassical quantum numbers (\hat{p}_z, θ_p, b) in the vortex core. Because of two nondegenerate branches (2), there are two sheets in the Fermi surface. One more representation of this is given in Fig. 3(d). It shows $b_{1,2}$ as a function of θ_p . The curves depend also on \hat{p}_z but that dependence is less important in the following because \hat{p}_z is conserved. For comparison, the trajectories passing precisely through the half cores at $y = \pm a/2$ would correspond to curves $b(\theta_p) = \mp \frac{1}{2}a \cos \theta_p$.

The topology of the effective Fermi surface is determined by the behavior of zero energy lines $b_{1,2}(\theta_p)$ at $\theta_p = \pi(n + 1/2)$ with $n = 1, 2$. At these angles the quasiparticle trajectories pass through both half cores. In general there is overlap of the quasiparticle wave functions localized at different half cores. This makes that there is no sign change of $b_{1,2}(\theta_b)$. That is, there is anticrossing of the two branches and a finite splitting $2\delta b = |b_1 - b_2| > 0$ at $\theta_p = \pi/2$, as shown by the solid lines in Fig. 3(d). Physically this means that an excitation created at one half core will jump periodically between the half cores.

The growing core separation (compared to ξ_0) at low temperatures and large pressures reduces the overlap of the quasiparticle wave functions located at different half cores. As a result the splitting $2\delta b$ becomes extremely small as shown by dashed lines in Fig. 3(d) for $F_1^s = 12$ and $T = 0.1T_c$. In this case *Landau-Zener* (LZ) tunneling between the quasiclassical branches (2) becomes important. The probability W of these transitions can be found from the conventional approach [35, 36] by taking θ_p and the angular momentum $\mu = p_\perp b$ as the conjugate variables. Near the anticrossing point at $\theta_p = \pi/2$ we can approximate $b_{1,2}(\theta_p) \approx \pm \sqrt{\delta b^2 + (a\theta/2)^2}$, where $\theta = \theta_p - \pi/2$. The transition probability is given by $W = \exp[-2k_\perp \text{Im} \int_0^{i\theta^*} (b_1 - b_2) d\theta]$ where $i\theta^* = 2i\delta b/a$ is the intersection point of quasiclassical branches in the complex plane. A simple calculation yields $W = \exp[-2\pi \hat{p}_\perp (\delta b / \Delta b)^2]$, where $\Delta b = \sqrt{a/k_F}$ has a physical meaning of the quantum mechanical uncertainty of the impact parameter.

Once the transition probability becomes large, $W \approx 1$, the LZ tunneling changes the topology of the effective Fermi surface so that quasiparticles remain localized in one or the other of the half cores. In Fig. 3(d) this means transition to intersecting zero energy curves $\tilde{b}_{1(2)}(\theta_p) = b_{1(2)}(\theta_p)$ for $-\pi/2 < \theta_p < \pi/2$ and $\tilde{b}_{1(2)}(\theta_p) = b_{2(1)}(\theta_p)$ for $\pi/2 < \theta_p < 3\pi/2$. The calculated LZ probability $W(T, P, \hat{p}_z)$ is shown in supplemental material [37] to demonstrate that the condition $W \approx 1$ is realized in the double-core vortex at large pressures and low temperatures. The crossover from split $b_{1,2}(\theta_p)$ to intersecting isoenergetic lines $\tilde{b}_{1,2}(\theta_p)$ is an analog of the *Lifshitz transition* [39] changing the topology of the Fermi surface.

The transition leads to a formation of two spatially separated low-energy fermionic states localized at the half-cores. Whether there are Majorana states precisely at the Fermi level [28] or not [27] is beyond our quasiclassical approach. The transition affects the rotational dynamics of the double-core vortex. The bound fermions in the core respond to oscillation of the core orientation. A friction torque acting on a rotating vortex core can be expressed by a friction coefficient $f = f_1 p_F (k_F \xi_0)^2$, where $f_1 \sim 1$ is dimensionless and the factor $p_F (k_F \xi_0)^2$ is determined by the density of quasiparticles in the vortex core. The expression for the friction torque [23] yields resonance peaks in f located at angular frequencies $\omega \approx n E_m / \hbar$ where n is integer. Here E_m is the spacing of quantized

	$P = 2$ bar	$P = 12$ bar	$P = 24$ bar
$T = 0.05T_c$	27 kHz	71 kHz	98 kHz
$T = 0.5T_c$	22 kHz	65 kHz	106 kHz

TABLE I: Values of the minigap E_m/h at different pressures and temperatures.

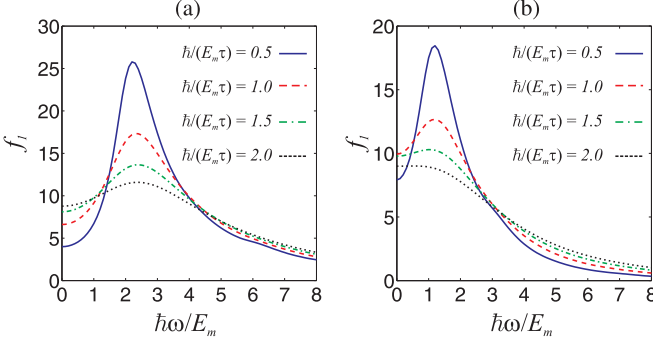


FIG. 4: (Color online) Demonstration of the effect of the Lifshitz transition on the rotational friction coefficient f_1 plotted as a function of frequency ω for (a) $W = 0$, (b) $W = 1$. The vortex structure and the excitation spectrum are calculated at $T = 0.5T_c$ and (a) $P = 2$ bar, (b) $P = 24$ bar. The minigap values are given in Table I. According to mutual friction measurements [12] $\hbar/E_m\tau = 0.7$ at $P = 24$ bar but a wider range is given to illustrate the influence of relaxation on the shape of absorption peak.

energy levels obtained from the quasiclassical spectrum (2) using the Bohr-Sommerfeld quantization rule for the angular momentum [23], $E_m = \hbar\langle\omega_1^{-1}(\hat{p}_z = 0)\rangle^{-1}$, where $\langle\ldots\rangle$ denotes the average over θ_p . The scale of the minigap is determined by $\hbar/\tau_n = (2\pi T_c)^2/v_F p_F$, which is on the order of the quasiparticle relaxation rate in the normal state. The calculated values of the minigap are listed in Table I.

The amplitudes of the resonances are determined by the Fourier amplitudes of the zero-energy curves shown in Fig. 3, $A_n \sim |\int d\theta_p e^{in\theta_p} b_1(\theta_p)|$. From the plots in Fig. 3(d) one can see that at pressures below the Lifshitz transition the largest components are those with double frequency $\hbar\omega = 2E_m$. At pressures above the transition the amplitudes are determined by the harmonics of the intersecting curves $\tilde{b}_i(\theta_p)$, which have strongest matrix element at $\hbar\omega = E_m$. The difference in the friction coefficient f_1 in the two cases is demonstrated in Fig. 4. In the following we show that at least the low frequency limit of the curves in Fig. 4 is experimentally accessible.

Kondo et al [13, 14] have studied a sample of rotating $^3\text{He-B}$ using the homogeneously precessing domain. In this mode the magnetization \mathbf{M} is tipped by a large angle ($> 104^\circ$) from the field direction \mathbf{B} . It was found that the contribution of vortices to the relaxation changed on a few minute time scale [13]. This was interpreted that

the double-core vortex gets twisted as its end points (at $z = \pm L/2$) are pinned but in the bulk the rotating magnetization exerts a torque on the core. A quantitative model was constructed for the vortex core rotation angle $\phi(t, z)$ as a function of time t and z . The parameters of the model were determined by fitting to the experiment [14]. These include the friction parameter f , the dipole torque T_D , which drives the vortex in the presence of rotating magnetization, and the rigidity K , which gives the energy caused by twisting the core, $F_{\text{twist}} = \frac{1}{2}K(\partial_z\phi)^2$.

By precise calculation of the vortex structure we can now calculate the vortex parameters. We find a value of f that is three orders of magnitude larger than fitted by Kondo et al [14]. Thus a serious revision of the model has to be made. The large value of f means that only a negligible fraction of energy dissipation comes from vortex core rotation. Thus essentially all dissipation has to arise from normal-superfluid disequilibrium [40], spin diffusion, and radiation of spin waves. Without going into details, these can be incorporated by allowing an elastic vortex structure, where the rotation angle $\alpha(t, z)$ at a distance from the vortex axis (where the dipole torque acts) can be different from the vortex core angle $\phi(t, z)$. These are bound by elasticity energy $\frac{1}{2}T_A(\alpha - \phi)^2$, and both angles have their own friction coefficients: $f\dot{\phi} = -\delta F/\delta\phi$, $g\dot{\alpha} = -\delta F/\delta\alpha$. This model results in the diffusion equation [37]

$$\dot{\phi} = \frac{K}{f}\partial_z^2\phi + \frac{P_g}{\omega f}, \quad (3)$$

where P_g is the power absorption per vortex length. An important virtue of this model is that based on our calculations of f and K , Eq. (3) predicts the time scale $L^2 f/\pi^2 K$ of several minutes. Thus Eq. (3) gives a simple explanation for the observed slow mode [13, 29, 30], which remained unexplained in previous models [14, 30].

In summary, we have investigated the spectrum of bound fermion states localized within the vortex core of weak-coupling p-wave superfluid. We predicted a Lifshitz transition, which separates low-energy quasiparticle states at the half cores and affects the rotational dynamics. Applying our results to Ref. 14 explains the observed long time scale and thus gives one more piece of evidence of the double-core nature of the low pressure vortex in $^3\text{He-B}$.

Acknowledgments

We thank I. Khaymovich, N. Kopnin, A. Mel'nikov, and G. Volovik for useful discussions. This work was supported by the Academy of Finland and Tauno Tönning foundation. M.S. and M.F. acknowledge support from the Swedish Research Council (VR).

-
- [1] R. Balian and N.R. Werthamer, Phys. Rev. **131**, 1553 (1963).
- [2] E.V. Thuneberg, Phys. Rev. Lett. **56**, 359 (1986).
- [3] M.M. Salomaa and G.E. Volovik, Phys. Rev. Lett. **56**, 363 (1986).
- [4] E.V. Thuneberg, Phys. Rev. B **36**, 3583 (1987).
- [5] G.E. Volovik, Pisma Zh. Eksp. Teor. Fiz. **52**, 972 (1990) [JETP Lett. **52**, 358 (1990)].
- [6] M. Fogelström and J. Kurkijärvi, J. Low Temp. Phys. **98**, 195 (1995), Erratum **100**, 597 (1995).
- [7] M. Fogelström and J. Kurkijärvi, J. Low Temp. Phys. **116**, 1 (1999).
- [8] T. Kita, Phys. Rev. B **66**, 224515 (2002).
- [9] O.T. Ikkala, G.E. Volovik, P.J. Hakonen, Yu.M. Bun'kov, S.T. Islander, G.A. Kharadze, Pis'ma Zh. Exp. Teor. Fiz. **35**, 338 (1982) [JETP Lett. **35**, 416 (1982)].
- [10] P.J. Hakonen, M. Krusius, M.M. Salomaa, J.T. Simola, Yu.M. Bunkov, V.P. Mineev and G.E. Volovik, Phys. Rev. Lett. **51**, 1362 (1983).
- [11] J.P. Pekola, J.T. Simola, P.J. Hakonen, M. Krusius, O.V. Lounasmaa, K.K. Nummila, G. Mamniashvili, R.E. Packard, G.E. Volovik, Phys. Rev. Lett. **53**, 584 (1984).
- [12] T.D.C. Bevan, A.J. Manninen, J.B. Cook, H. Alles, J.R. Hook and H.E. Hall, J. Low Temp. Phys. **109** 423 (1997).
- [13] V.V. Dmitriev, Y. Kondo, J.S. Korhonen, M. Krusius, Yu.M. Mukharskiy, E.B. Sonin, and G.E. Volovik, Physica B **165&166**, 655 (1990).
- [14] Y. Kondo, J.S. Korhonen, M. Krusius, V.V. Dmitriev, Y.M. Mukharsky, E.B. Sonin, and G.E. Volovik, Phys. Rev. Lett. **67**, 81 (1991).
- [15] Y. Tsutsumi, K. Machida, T. Ohmi, and M. Ozaki, J. Phys. Soc. Jpn. **81**, 074717 (2012).
- [16] C. Caroli, P. G. de Gennes, J. Matricon, Phys. Lett. **9**, 307 (1964).
- [17] J. Bardeen, R. Kümmel, A.E. Jacobs, and L. Tewordt, Phys. Rev. **187**, 556 (1969).
- [18] A.I. Larkin, Yu.N. Ovchinnikov, Phys. Rev. B **57**, 5457 (1998).
- [19] D. Rainer, J.A. Sauls, and D. Waxman, Phys. Rev. B **54**, 10094 (1996).
- [20] M. Stone, Phys. Rev. B **54**, 13 222 (1996).
- [21] N.B. Kopnin, Rep. Prog. Phys. **65**, 1633 (2002).
- [22] N. Nakai, P. Miranovic, M. Ichioka, and K. Machida, Phys. Rev. B **73**, 172501 (2006).
- [23] N.B. Kopnin and G.E. Volovik, Phys. Rev. B **57**, 8526 (1998).
- [24] M.A. Silaev, G.E. Volovik, J. Low Temp. Phys. **161**, 460 (2010).
- [25] M.A. Silaev, G.E. Volovik, JETP, **119**, 1042, (2014).
- [26] T. Mizushima, Y. Tsutsumi, M. Sato, and K. Machida, J. Phys.: Condens. Matter **27**, 113203 (2015).
- [27] Y. Tsutsumi, T. Kawakami, K. Shiozaki, M. Sato, and K. Machida, Phys. Rev. B **91**, 144504 (2015).
- [28] D.A. Ivanov, Phys. Rev. Lett. **86**, 268 (2001).
- [29] E.B. Sonin, Y. Kondo, J.S. Korhonen, and M. Krusius, Europhys. Lett. **22**, 125 (1993).
- [30] M. Krusius, J.S. Korhonen, Y. Kondo, and E.B. Sonin, Phys. Rev. B **47**, 15113 (1993).
- [31] J.W. Serene and D. Rainer, Phys. Rep. **101**, 221 (1983).
- [32] D.S. Greywall, Phys. Rev. B **33**, 7520 (1986).
- [33] A.F. Andreev, Zh. Exp. Teor. Fiz. **46**, 1823 (1964) [Sov. Phys. JETP **19**, 1228 (1964)].
- [34] M.A. Silaev, Pis'ma Zh. Exp. Teor. Fiz. **90**, 433 (2009) [JETP Lett. **90**, 391 (2009)].
- [35] L.D. Landau and E.M. Lifshitz, *Quantum Mechanics*, Pergamon Press (1965).
- [36] A.S. Mel'nikov, D.A. Ryzhov, M.A. Silaev, Phys. Rev. B **78**, 064513 (2008).
- [37] See Supplemental Material at <http://> , which includes Ref. [38].
- [38] E.V. Thuneberg, J. Low Temp. Phys. **122**, 657 (2001).
- [39] I.M. Lifshitz, Sov. Phys. JETP **11**, 1130 (1960).
- [40] A.J. Leggett and S. Takagi, Ann. Phys. (New York) **106**, 79 (1977).

SUPPLEMENTAL MATERIAL

Lifshitz transition in the double-core vortex in $^3\text{He-B}$

I. LANDAU-ZENER TUNNELING PROBABILITY BETWEEN THE QUASICLASSICAL SPECTRUM BRANCHES

The topology of quasiparticle spectrum in double-core vortices is determined by the behavior of quasiclassical spectrum branches $\varepsilon = \varepsilon_{1,2}(\hat{p}_z, \theta_p, b)$ near the intersection points at $\theta_p = \pi/2 + \pi n$, see Fig. 3(d) in the main text. In the Fig. 5 we show in detail these curves in the vicinity of an anticrossing point $\theta_p = \pi/2$ for several values of parameters. This plot illustrates main properties of the splitting δb as function of temperature T , pressure P , momentum projection to the vortex axis \hat{p}_z .

Quantitatively the splitting δb is determined by the overlap between quasiparticle wave functions localized at different half-cores as shown in the Fig. 1 in the main text. At low temperatures the characteristic localization scale is determined by the coherence length ξ_0 . On the other hand the distance between vortex cores a is determined by the scale $R_0 = (1 + F_1^s)\xi_0$ so that the ratio R_0/ξ_0 increases with growing pressure. Hence the overlap at large pressures is weaker and the splitting δb decreases as can be seen comparing the curves for $F_1^s = 9$ ($P = 11.6$ bar) and $F_1^s = 12$ ($P = 23.75$ bar) in Fig. 5(a). At larger temperatures the quasiparticle localization is determined by the temperature-dependent coherence length $\xi \approx \hbar v_F/\Delta$ where $\Delta = \Delta(T)$ is the gap amplitude. On the other hand the distance between vortex cores for temperatures up to $T = 0.99T_c$ has a much weaker temperature dependence for $F_1^s = 6, 9, 12$ as shown in Fig. 2 in the main text. Thus the overlap between half-core states and the splitting δb strongly decrease with decreasing temperature which can be seen from the comparison of the curves $b = b_{1,2}(\theta_p)$ for $T = 0.9T_c$ and $0.1T_c$ in Fig. 5(b).

The most striking is the dependence of splitting δb on the quasiparticle momentum projection on the vortex axis \hat{p}_z . The absolute value of momentum is fixed and determined by the Fermi momentum. Hence different values of \hat{p}_z correspond to the different angles of quasiclassical trajectories with respect to the vortex axis. For the finite \hat{p}_z the effective distance between half-cores *along the trajectories* is elongated by the factor of $1/\sqrt{1 - \hat{p}_z^2}$ which decreases the overlap of localized states and suppresses the splitting δb . As can be seen in Figs. 5(c) and 5(d), the splitting can decrease to the very small values at large $\hat{p}_z \sim 1$.

The splitting δb determines the tunneling between the quasiclassical branches. The Landau-Zener tunneling probability $W = W(T, P, \hat{p}_z)$ calculated according to the general expression from the main text is shown in Figs. 6(a) and 6(b) as function of temperature for several values of P and \hat{p}_z . These curves demonstrate a general tendency of the tunneling probability to increase with decreasing temperatures and increasing pressure. The probability is strongly enhanced at large \hat{p}_z . Thus the Lifshitz transition determined by $W \sim 1$ occurs at different values of P and T for different \hat{p}_z . From Fig. 6 one can see that at high pressures and low temperatures the condition $W \sim 1$ is valid for all values of \hat{p}_z .

II. MODEL OF ROTATIONAL DYNAMICS

The rotational dynamics of the double-core vortex was studied by Kondo et al [14]. Here we present a modified model that allows azimuthal shear of the vortex structure. Such a case appears because the driving dipole torque acts on the asymptotic order parameter, typically a distance $\xi_D \approx 10 \mu\text{m}$ from the vortex axis, whereas the opposing rotational friction occurs in the vortex cores, on the scale of coherence length $\xi_0 \approx 10 \text{ nm}$. Our notation follows closely Ref. 14 and the model of Ref. 14 is obtained in the limiting case $T_A \rightarrow \infty$ and $g = 0$.

We study the model where the free energy of a single vortex parallel to z is

$$F = \int dz \left[-T_H(\hat{S}_\alpha R_{\alpha i} \hat{b}_i)^2 + T_D(\hat{\mathbf{a}} \cdot \hat{\mathbf{n}})^2 - T_A(\hat{\mathbf{a}} \cdot \hat{\mathbf{b}})^2 + \frac{1}{2}K(\partial_z \phi)^2 \right] \quad (4)$$

The magnetic field term (coefficient T_H) depends on the hard core anisotropy axis $\hat{\mathbf{b}} = \hat{\mathbf{x}} \cos \phi + \hat{\mathbf{y}} \sin \phi$. The dipole term (coefficient T_D) depends on the soft core anisotropy axis $\hat{\mathbf{a}} = \hat{\mathbf{x}} \cos \alpha + \hat{\mathbf{y}} \sin \alpha$. The azimuthal shear term (coefficient T_A) is supposed to be strong enough to keep the two anisotropy vectors nearly parallel. Other quantities are the spin-orbit rotation matrix $R_{\alpha i}$ parametrized by axis $\hat{\mathbf{n}} = \hat{\mathbf{y}} \cos \omega t + (\hat{\mathbf{z}} \sin \eta - \hat{\mathbf{x}} \cos \eta) \sin \omega t$ and angle $\theta = \arccos(-1/4)$, the direction of the precessing magnetization $\hat{S}_\alpha = R_{\alpha i} \hat{H}_i$, and the static field $\mathbf{H} = H(\hat{\mathbf{x}} \sin \eta + \hat{\mathbf{z}} \cos \eta)$. This model neglects the anisotropy of the dipole energy in the double-core vortex in the plane perpendicular to $\hat{\mathbf{a}} \approx \hat{\mathbf{b}}$. In principle, we should allow $\hat{\mathbf{a}}$ to have component in the z direction also, but this will not affect the main results and thus is

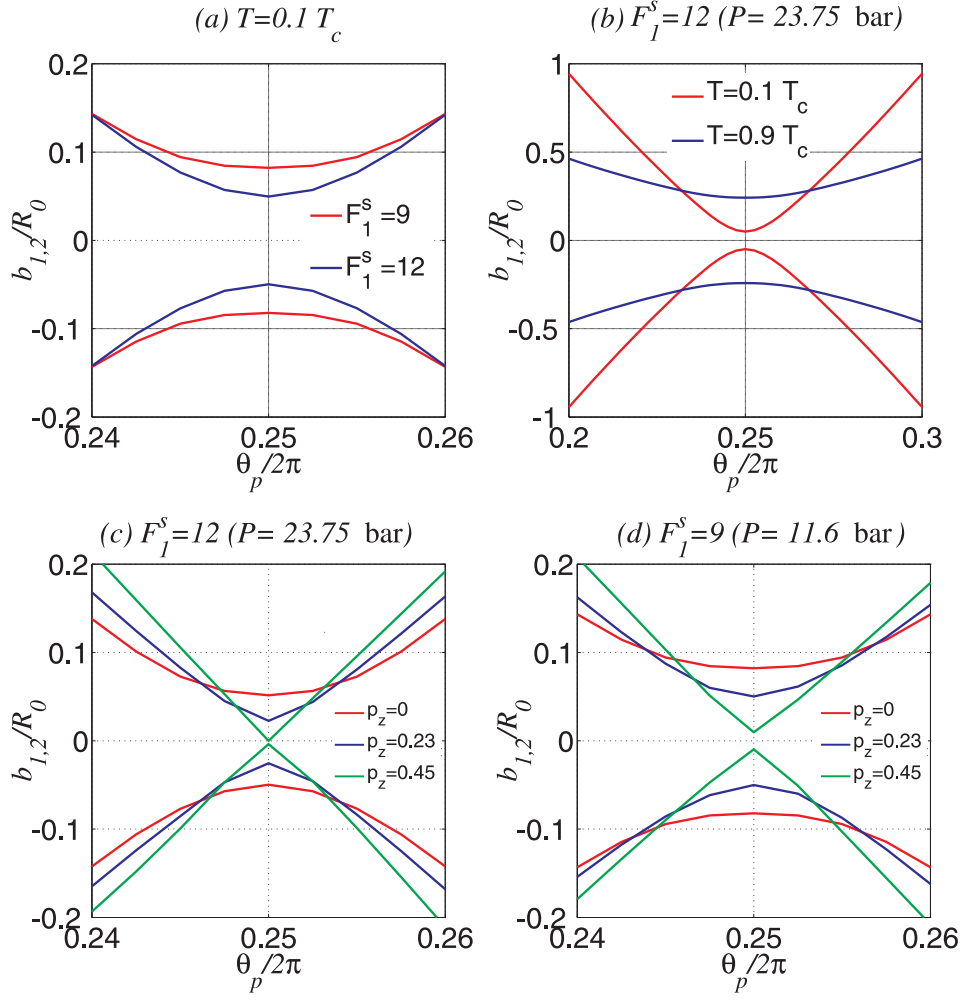


FIG. 5: (Color online) Detailed structure of zero-energy lines $b = b_{1,2}(\theta_p)$ near the anticrossing point $\theta_p = \pi/2$ for different values of parameters. (a) $T = 0.1 T_c$ and different values of pressure $F_1^s = 9$ (red), $F_1^s = 12$ (blue); (b) $F_1^s = 12$ and $T = 0.9 T_c$ (blue), $T = 0.1 T_c$ (red); (c) $F_1^s = 12$, (d) $F_1^s = 9$ and different momentum projections $\hat{p}_z = 0$ (red), 0.23 (blue), 0.45 (green).

dropped here for simplicity. We get

$$\begin{aligned}
 F &= \int dz \left[-T_H(\hat{\mathbf{H}} \cdot \hat{\mathbf{b}})^2 + T_D(\hat{\mathbf{a}} \cdot \hat{\mathbf{n}})^2 - T_A(\hat{\mathbf{a}} \cdot \hat{\mathbf{b}})^2 + \frac{1}{2}K(\partial_z \phi)^2 \right] \\
 &= \int dz \left[-T_H \sin^2 \eta \cos^2 \phi + T_D(\cos \omega t \sin \alpha - \cos \eta \sin \omega t \cos \alpha)^2 + T_A(\alpha - \phi)^2 + \frac{1}{2}K(\partial_z \phi)^2 \right]
 \end{aligned} \tag{5}$$

Note that for $\hat{\mathbf{H}} = \hat{\mathbf{x}}$, $\cos \eta = 0$ and both field and dipole terms are minimized by $\phi = \alpha = n\pi$, that is $\hat{\mathbf{a}} = \hat{\mathbf{b}} = \pm \hat{\mathbf{x}}$ and $\hat{\mathbf{n}}$ rotating around it.

We suppose the frictional equations of motion

$$g\dot{\alpha} = -\frac{\delta F}{\delta \alpha}, \quad f\dot{\phi} = -\frac{\delta F}{\delta \phi}. \tag{6}$$

We obtain

$$g\dot{\alpha} = -\frac{\delta F}{\delta \alpha} = -T_D \sin^2 \omega t \sin^2 \eta \sin 2\alpha - T_D \cos 2\omega t (1 - \cos \eta) \sin 2\alpha + T_D \cos \eta \sin 2(\omega t - \alpha) - 2T_A(\alpha - \phi). \tag{7}$$

Using the same approximation as Kondo et al this simplifies to

$$g\dot{\alpha} = -\frac{1}{2}T_D \sin^2 \eta \sin 2\alpha + T_D \cos \eta \sin 2(\omega t - \alpha) - 2T_A(\alpha - \phi). \tag{8}$$

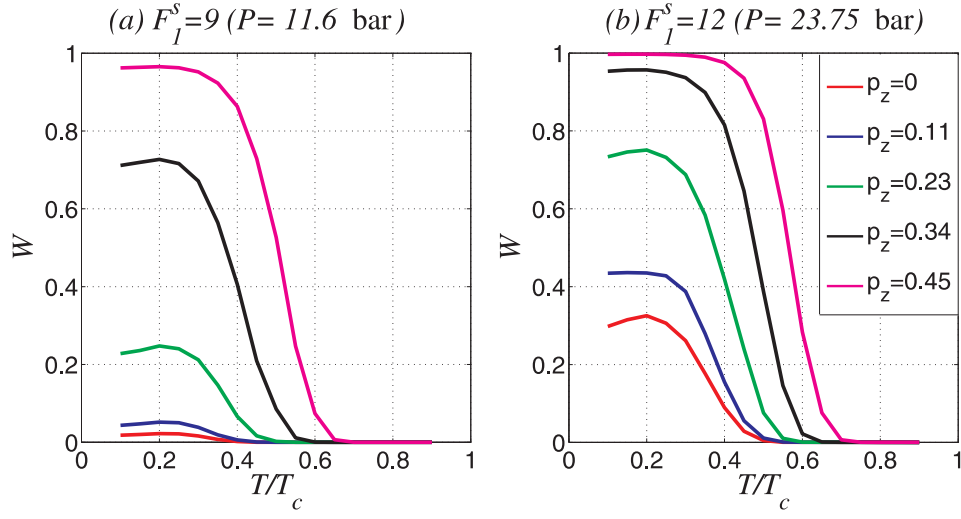


FIG. 6: (Color online) Temperature dependencies of the Landau-Zener tunneling probability between quasiclassical spectral branches in the double-core vortex for (a) $F_1^s = 9$ ($P = 11.6$ bar), (b) $F_1^s = 12$ ($P = 23.75$ bar) and different values of momentum projection \hat{p}_z .

This expression is exact in second (but not fourth) power in η . The other equation is

$$f\dot{\phi} = -\frac{\delta F}{\delta \phi} = -T_H \sin^2 \eta \sin 2\phi + 2T_A(\alpha - \phi) + K\partial_z^2 \phi. \quad (9)$$

Suppose now that f is very large, which means $\phi(t)$ is so slow that it can be taken as a constant during one cycle. We study

$$g\dot{\alpha} = -M \sin 2\alpha + G \sin 2(\omega t - \alpha) - 2T_A(\alpha - \phi) \quad (10)$$

where in the approximation above $M = \frac{1}{2}T_D \sin^2 \eta$ and $G = T_D \cos \eta$. Suppose $\alpha(t) = \alpha_0 + \alpha_1(t)$ with small α_1

$$g\dot{\alpha}_1 = -M \sin 2\alpha_0 - 2T_A(\alpha_0 - \phi) + G \sin 2(\omega t - \alpha_0) - 2(T_A + M \cos 2\alpha_0)\alpha_1 - 2G \cos 2(\omega t - \alpha_0)\alpha_1. \quad (11)$$

Assuming $\alpha_1 = A \cos 2(\omega t - \chi)$

$$\begin{aligned} & -2\omega g A \sin 2(\omega t - \chi) \\ & = -M \sin 2\alpha_0 - 2T_A(\alpha_0 - \phi) + G \sin 2(\omega t - \alpha_0) - 2A(T_A + M \cos 2\alpha_0) \cos 2(\omega t - \chi) \\ & \quad - GA \cos 2(2\omega t - \alpha_0 - \chi) - GA \cos 2(\chi - \alpha_0). \end{aligned} \quad (12)$$

At frequencies 0 and 2ω we get

$$\begin{aligned} 0 & = -M \sin 2\alpha_0 - 2T_A(\alpha_0 - \phi) - GA \cos 2(\chi - \alpha_0) \\ -2\omega g A \sin 2(\omega t - \chi) & = G \sin 2(\omega t - \alpha_0) - 2A(T_A + M \cos 2\alpha_0) \cos 2(\omega t - \chi) \end{aligned} \quad (13)$$

The latter equation can be written

$$2A(T_A + M \cos 2\alpha_0) \cos 2(\omega t - \chi) - 2\omega g A \sin 2(\omega t - \chi) = G \sin 2(\omega t - \alpha_0) \quad (14)$$

$$\begin{aligned} 2A(T_A + M \cos 2\alpha_0) \cos 2\omega t - 2\omega g A \sin 2\omega t & = G \sin 2(\omega t + \chi - \alpha_0) \\ & = G[\sin 2\omega t \cos 2(\chi - \alpha_0) + \cos 2\omega t \sin 2(\chi - \alpha_0)] \end{aligned} \quad (15)$$

$$\begin{aligned} 2A(T_A + M \cos 2\alpha_0) & = G \sin 2(\chi - \alpha_0) \\ -2\omega g A & = G \cos 2(\chi - \alpha_0) \end{aligned} \quad (16)$$

$$A^2 = \frac{G^2/4}{\omega^2 g^2 + (T_A + M \cos 2\alpha_0)^2} \approx \frac{G^2/4}{\omega^2 g^2 + T_A^2} = \frac{\frac{1}{4}T_D^2 \cos^2 \eta}{\omega^2 g^2 + T_A^2}. \quad (17)$$

The absorbed power is determined by A ,

$$P_g = -\langle \dot{\alpha} \frac{\delta F}{\delta \alpha} \rangle = g \langle \dot{\alpha}^2 \rangle = 2g\omega^2 A^2. \quad (18)$$

Note that here P denotes the absorption per vortex length whereas in Ref. 14 P denotes the total absorption.

Applying the latter of (16) to the first equation (13) gives

$$M \sin 2\alpha_0 + 2T_A(\alpha_0 - \phi) - 2\omega g A^2 = 0. \quad (19)$$

From (9) we have

$$f \dot{\phi} = -T_H \sin^2 \eta \sin 2\phi + 2T_A(\alpha_0 - \phi) + K \partial_z^2 \phi. \quad (20)$$

Because ϕ is a slow variable, it is only the low frequency limit of f that appears. What remains to be solved is ϕ and α_0 from equations (19) and (20). Two different cases need to be studied.

1) Rocking oscillations. We assume a solution where the left hand side of (20) vanishes,

$$-\frac{\delta F}{\delta \phi} = -T_H \sin^2 \eta \sin 2\phi + 2T_A(\alpha_0 - \phi) + K \partial_z^2 \phi = 0. \quad (21)$$

Supposing $\phi - \alpha \ll 1$ we can solve this

$$\phi = \alpha_0 - \frac{T_H \sin^2 \eta \sin 2\alpha_0 - K \partial_z^2 \alpha_0}{2(T_H \sin^2 \eta \cos 2\alpha_0 + T_A)} \approx \alpha_0 - \frac{T_H \sin^2 \eta \sin 2\alpha_0 - K \partial_z^2 \alpha_0}{2T_A}. \quad (22)$$

The lag of ϕ behind α_0 is an increasing function of $\phi \approx \alpha_0$ for $0 < \phi \approx \alpha_0 < \pi/4$. Substituting (22) into (19) gives

$$(T_H + \frac{1}{2}T_D) \sin^2 \eta \sin 2\alpha_0 - K \partial_z^2 \alpha_0 - 2\omega g A^2 = 0 \quad (23)$$

and thus

$$\sin 2\alpha_0 = \frac{2\omega g A^2 + K \partial_z^2 \alpha_0}{(T_H + \frac{1}{2}T_D) \sin^2 \eta}. \quad (24)$$

This solution is possible only if the right hand side of (24) is less than unity. At equality, $\alpha_0 = \pi/4 + n\pi$. The stability condition at $\partial_z^2 \alpha_0 = 0$ can be written

$$\tan^2 \eta > \tan^2 \eta_0 = \frac{\frac{1}{2}\omega g T_D^2}{(T_H + \frac{1}{2}T_D)(\omega^2 g^2 + T_A^2)}. \quad (25)$$

Interestingly, this can also be written

$$\sin^2 \eta > \sin^2 \eta_0 = \frac{P_g}{\omega(T_H + \frac{1}{2}T_D)}. \quad (26)$$

These results are essentially ($\tan \eta_0 \approx \sin \eta_0$) the same as in Ref. 14 if one makes the replacement $f \rightarrow g + T_A^2/g\omega^2$.

2) In the case solution (24) is not possible, we get slow rolling motion of $\phi(t)$. For simplicity we consider $\eta = 0$ only. From (19) we get

$$2T_A(\alpha_0 - \phi) = 2\omega g A^2 \quad (27)$$

and substitution to (20) gives

$$\dot{\phi} = \frac{K}{f} \partial_z^2 \phi + \frac{P_g}{\omega f}. \quad (3)$$

Equation (3) is a diffusion equation

$$\dot{\phi} = D \partial_z^2 \phi + C \quad (28)$$

The solution for $0 < z < L$ and $t > 0$ with boundary conditions $\phi(z = 0) = 0 = \phi(z = L)$ can be found as Fourier series

$$\phi = \frac{C}{2D}(Lz - z^2) + \sum_n B_n e^{-Dk_n^2 t} \sin k_n z \quad (29)$$

with $k_n = n\pi/L$. The slowest component has the rate

$$\Gamma = \pi^2 D/L^2 = \pi^2 K/fL^2. \quad (30)$$

We compare our results to Ref. 14. For that we give numerical values of our weak-coupling results corresponding to 29.3 bars pressure, $T/T_c = 0.5$ and $L = 7$ mm. At this pressure $F_1^s = 13.3$ and we neglect other Fermi-liquid interactions. For the friction coefficient we get $f \approx 2 \times 10^{-19}$ J s/m, see Section III. In section IV we calculate $K \approx 5 \times 10^{-27}$ Jm. This gives the time constant $\Gamma^{-1} \approx 3$ min. This order of magnitude is in good agreement with the measured value of the “slow mode” in Ref. 13, 29, 30. Extensive measurements of the slow mode are presented in Ref. 30. It seems that these results need to be reinterpreted using the diffusion equation (3).

Our results could be compared to $f = 4.5 \times 10^{-23}$ J s/m and $K = 1.1 \times 10^{-25}$ Jm that were obtained by fitting the experiment to the model in Ref. 14.

III. ROTATIONAL FRICTION

The calculation of the rotational friction coefficient f in the main text applies the kinetic equation of Ref. 23 to our numerical solution of the excitation spectrum in the vortex core. The results are presented in Fig. 4. Evaluating this at the conditions of Ref. 14 (see above) gives $f = 1.7 \times 10^{-19}$ J s/m in the low frequency limit. The result at the Larmor precession frequency at $H = 14.2$ mT ($\hbar\omega/E_m = 3.9$) would be $f(\omega_L) = 0.9 \times 10^{-19}$ J s/m.

An alternative estimate of f is obtained as follows. In the case of strong Landau-Zener tunneling, the half cores behave as separated half-quantum vortices except that they are bound together at the distance a . The standard mutual friction force [12, 21] applied to both half cores gives

$$f = \frac{1}{4} a^2 \kappa \rho_s d_{\parallel}, \quad (31)$$

where $\kappa = \pi\hbar/m$ is the circulation quantum, ρ_s the superfluid density and d_{\parallel} the mutual friction parameter. Taking a from Fig. 2 and d_{\parallel} from Ref. 12 gives $f = 1.6 \times 10^{-19}$ J s/m at the conditions stated above.

IV. TWIST RIGIDITY

The twisting of a double-core vortex is measured by a twist wave vector $k = \partial_z \phi$. For a small twist the additional free energy is supposed to be quadratic in k ,

$$F_{\text{twist}} = \frac{1}{2} K k^2. \quad (32)$$

Here we aim to calculate the twist-rigidity coefficient K .

The reduced order parameter is expected to satisfy the boundary condition $\tilde{\mathbf{A}}(r, \varphi, z) \rightarrow \mathbf{l} e^{i\varphi}$ for $r \rightarrow \infty$, where \mathbf{l} is a unit matrix. An axially symmetric vortex satisfies the following symmetry [4]

$$\tilde{\mathbf{A}}(r, \phi) = e^{i\theta} \mathbf{R}(\hat{\mathbf{z}}, \theta) \tilde{\mathbf{A}}(r, \phi - \theta) \mathbf{R}(\hat{\mathbf{z}}, -\theta), \quad (33)$$

where \mathbf{R} is a rotation matrix parametrized by an axis and angle of rotation. A twisted vortex apparently has the property

$$\tilde{\mathbf{A}}(r, \phi, z) = e^{ikz} \mathbf{R}(\hat{\mathbf{z}}, kz) \tilde{\mathbf{A}}(r, \phi - kz, 0) \mathbf{R}(\hat{\mathbf{z}}, -kz). \quad (34)$$

Taking the z derivative and evaluating it at $z = 0$ gives

$$\frac{\partial \tilde{\mathbf{A}}}{\partial z} = k \mathbf{B}, \quad (35)$$

where

$$\mathbf{B} = i\tilde{\mathbf{A}} + \mathbf{R}'\tilde{\mathbf{A}} - \tilde{\mathbf{A}}\mathbf{R}' + y\frac{\partial\tilde{\mathbf{A}}}{\partial x} - x\frac{\partial\tilde{\mathbf{A}}}{\partial y}, \quad \mathbf{R}' = \begin{pmatrix} 0 & -1 & 0 \\ 1 & 0 & 0 \\ 0 & 0 & 0 \end{pmatrix}. \quad (36)$$

In the Ginzburg-Landau region the twist-rigidity coefficient K is given by

$$K = 2\lambda_{G2} \int d^2r \sum_{\mu=1}^3 \left[\sum_{j=1}^3 |B_{\mu j}|^2 + 2|B_{\mu z}|^2 \right]. \quad (37)$$

In order to get a good approximation of the twist rigidity at general temperature, we have written the prefactor using [38]

$$\lambda_{G2} = \frac{\hbar^2 \rho (1 - Y)}{40 m m^*}. \quad (38)$$

This form of λ_{G2} is valid since we assume $F_1^a = F_3^a = 0$. Physically, the twisting (34) causes axial spin flow in the asymptotic region and axial mass flow in the vortex center, but the F_1^a dependence of the former and the F_1^s dependence of the latter are not properly included in (37).

The asymptotic form of the order parameter (neglecting dipole-dipole coupling) far from the vortex axis is of the form $\tilde{\mathbf{A}} = \mathbf{R}(\boldsymbol{\theta}) + O(r^{-2})$, where

$$\boldsymbol{\theta} = \frac{C_1 \cos \phi}{r} \left(\frac{\sin \phi}{1+c} \hat{\mathbf{r}} + \cos \phi \hat{\boldsymbol{\phi}} \right) + \frac{C_2 \sin \phi}{r} \left(-\frac{\cos \phi}{1+c} \hat{\mathbf{r}} + \sin \phi \hat{\boldsymbol{\phi}} \right). \quad (39)$$

In general $c = \lambda_{G1}/2\lambda_{G2}$ but in the present approximation $F_1^a = F_3^a = 0$ we have $c = 1$ [38]. Based on this, we can calculate the asymptotic contribution to the twist rigidity. Since (39) is expressed in cylindrical coordinates, the twist energy can be calculated more directly than above, by replacing ϕ by $\phi - kz$. The additional energy can be evaluated from the gradient energy [38]

$$\begin{aligned} F_{Gz} &= 2\lambda_{G2}(1+c) \int d^2r \frac{\partial\theta_k}{\partial z} \frac{\partial\theta_k}{\partial z} = 2\lambda_{G2}(1+c)k^2 \int d^2r \frac{\partial\theta_k}{\partial\phi} \frac{\partial\theta_k}{\partial\phi} \\ &= 2\lambda_{G2}(1+c)k^2 \int d\phi \int dr \frac{1}{r} \left[\frac{(\cos^2 \phi - \sin^2 \phi)^2}{(1+c)^2} + 4\cos^2 \phi \sin^2 \phi \right] (C_1 - C_2)^2 \\ &= 2\pi\lambda_{G2}k^2 \frac{2+2c+c^2}{1+c} (C_1 - C_2)^2 \int dr \frac{1}{r}. \end{aligned} \quad (40)$$

Comparison to (32) allows to identify

$$K_{\text{tail}} = 4\pi\lambda_{G2} \frac{2+2c+c^2}{1+c} (C_1 - C_2)^2 \int dr \frac{1}{r}. \quad (41)$$

The dipole-dipole energy suppresses the contribution at distances beyond the dipole length ξ_d .

We estimate numerical values under conditions explained above [below Eq. (30)]. Substituting the numerical order parameter into (37) gives $K = 3.2 \times 10^{-27}$ Jm in the region $r < 60\xi_0$. Adding the asymptotic part from (41) with $C_1 = 3.7R_0$ and $C_2 = 0.1R_0$ we get $K = 4.0 \times 10^{-27}$ Jm.

Another estimation of the twist rigidity is to calculate the twisting energy of a pair of half-quantum vortices. Estimating energy by the length increase of the twisted pair gives

$$K_{\text{mass flow}} = \frac{\rho_s \kappa^2 a^2}{32\pi} \ln \frac{a}{r_c} \quad (42)$$

where a is the distance between the half cores and r_c their radius. Estimating $a = 5.4R_0$ gives $K_{\text{mass flow}} = 1.9 \times 10^{-27}$ Jm. Estimating this without Fermi-liquid interaction, i.e. as we did in (37), we would get $K_{\text{mass flow}0} = 0.6 \times 10^{-27}$ Jm. Supposing this difference is just missing in the formula based on (37), the corrected value for total twist coefficient is $K = 5.3 \times 10^{-27}$ Jm.